online data

The inositol 1,4,5-trisphosphate receptor (*Itpr*) gene family in *Xenopus*: identification of type 2 and type 3 inositol 1,4,5-trisphosphate receptor subtypes

Dan ZHANG[1], Michael J. BOULWARE[1], Matthew R. PENDLETON, Taisaku NOGI and Jonathan S. MARCHANT[2]

Department of Pharmacology, University of Minnesota Medical School, MN 55455, U.S.A.

Studies in the *Xenopus* model system have provided considerable insight into the developmental role of intracellular Ca^{2+} signals produced by activation of IP_3Rs (inositol 1,4,5-trisphosphate receptors). However, unlike mammalian systems where three IP_3R subtypes have been well characterized, our molecular understanding of the IP_3Rs that underpin Ca^{2+} signalling during *Xenopus* embryogenesis relate solely to the original characterization of the '*Xenopus* IP_3R' cloned and purified from *Xenopus laevis* oocytes several years ago. In the present study, we have identified *Xenopus* type 2 and type 3 IP_3Rs and report the full-length sequence, genomic architecture and developmental expression profile of these additional IP_3R subtypes. In the light of the emerging genomic resources and opportunities for genetic manipulation in the diploid frog *Xenopus tropicalis*, these data will facilitate manipulations to resolve the contribution of IP_3R diversity in Ca^{2+} signalling events observed during vertebrate development.

Key words: Ca^{2+} channel, Ca^{2+} signalling, inositol 1,4,5-trisphosphate (IP_3), inositol 1,4,5-trisphosphate receptor (IP_3R), *Xenopus*.

INTRODUCTION

Studies in the *Xenopus* model system have proved to be of great utility in providing information about the cellular organization, properties and function of IP_3Rs [IP_3 (inositol 1,4,5-trisphosphate) receptors]. As a biophysical 'test tube' amenable to heterologous expression, biochemistry, live-cell imaging and electrophysiology, *Xenopus* oocytes have proved to be a facile system in which to resolve, manipulate and model intracellular Ca^{2+} signals evoked by IP_3. Early studies using *Xenopus* oocytes demonstrated key features of subcellular IP_3R organization and regulation within their native environment that are conserved in mammalian systems [1], as well as principles of Ca^{2+} signal initiation and propagation that establish discrete spatiotemporal profiles of Ca^{2+} signals that are crucial for activating specific cellular responses [2]. Furthermore, the tractability of the *Xenopus* system for embryological analysis has provided considerable insight into the cell biological role of IP_3Rs during maturation [3–7], fertilization [3], cleavage [8] and early embryonic patterning (including a crucial role in dorsoventral axis formation [9]).

In contrast with our functional understanding of the role of IP_3R-mediated Ca^{2+} release in these events, our molecular knowledge of the '*Xenopus* IP_3R' derives solely from the original studies detailing the purification [10] and cloning [3] of a single (type 1) IP_3R from *Xenopus laevis* oocytes reported well over a decade ago (reviewed in [11]). In mammals, three IP_3R subtypes [12–14], as well as multiple splice variants (IP_3R1 and IP_3R2 [15–17]), have been well characterized. Such molecular diversity in the mammalian *Itpr* (IP_3R) gene family is likely to be significant in customizing Ca^{2+} signals to cellular function through modulation of the sensitivity and regulatory susceptibility of cellular IP_3Rs [16,18–20] and hence the spatiotemporal profile of cytoplasmic Ca^{2+} signals [15,21,22]. Indeed, expression analysis during primary tissue differentiation verifies a changing cellular complement of IP_3Rs that probably heralds developmental significance [15,23] in the light of specific functional roles for discrete IP_3R subtypes [24–26].

In the present study, we set out to characterize the molecular diversity of the *Xenopus* IP_3R family and describe (i) the full-length sequence of *Xenopus tropicalis* type 2 (*Xt*-IP_3R2) and type 3 (*Xt*-IP_3R3) IP_3R subtypes, (ii) their developmental expression profile, and (iii), by exploiting the emerging genome sequence of *X. tropicalis*, the genomic architecture of the *Itpr* gene family in this important vertebrate model organism. Finally, as this work completes the first *in vivo* characterization of the full-length sequence of three IP_3R subtypes outside a mammalian model system [3], we speculate on the diversification of the *Itpr* gene family during vertebrate evolution.

MATERIALS AND METHODS

Xenopus husbandry

Adult *Xenopus* frogs (NASCO) were killed, and tissues were surgically removed for subsequent RNA extraction. For preparation of mRNA from oocytes, pigmented stage VI *Xenopus* oocytes were harvested from ovarian lobes and isolated by defolliculation [27]. Epithelial cell layers were removed manually using watchmaker's forceps, and then oocytes were briefly exposed to 0.5 mg/ml type I collagenase (Sigma) for removal of follicular cells. *Xenopus* embryos were obtained by artificial fertilization, and subsequently de-jellied and maintained in

Abbreviations used: IP_3, inositol 1,4,5-trisphosphate; IP_3R, IP_3 receptor; *Itpr* gene, IP_3R gene; MBT, mid-blastula transition; ODC, ornithine decarboxylase; ORF, open reading frame; RT, reverse transcription; UTR, untranslated region; WGD, whole-genome duplication; *Xbra, Xenopus* brachyury; *Xt*, *Xenopus tropicalis*.

[1] These authors contributed equally to this work.

[2] To whom correspondence should be addressed (email march029@umn.edu).

The nucleotide sequence data reported will appear in the DDBJ, EMBL, GenBank® and GSDB Nucleotide Sequence Databases under the accession numbers EF507433 (*Iptr2*) and EF507432 (*Iptr3*).

0.3× MMR (1.5 mM Hepes, 30 mM NaCl, 0.6 mM KCl, 0.3 mM $MgCl_2$ and 0.6 mM $CaCl_2$, pH 7.8).

RT (reverse transcription)–PCR analysis and sequencing

Total RNA was prepared from ~30 *Xenopus* embryos, or specific adult tissue sources, using TRIzol® (Invitrogen). cDNA was reverse-transcribed using the SuperScript™ III First-Strand Synthesis System (Invitrogen) according to the manufacturer's instructions, using anchor dT, random hexamer or transcript-specific primers. To identify the complete ORF (open reading frame) of the IP_3R subtypes, a variety of primer sets were employed (summarized in Supplementary Table 3 at http://www.BiochemJ.org/bj/404/bj4040383add.htm), and products were amplified using either GoTaq® Green Master Mix (Promega), Takara LA Taq™ or Speedstar HS Polymerase. Amplified fragments were cloned into the pGEM-T Easy vector (Promega), sequenced (University of Minnesota, Biomedical Genomics Center) and assembled using ContigExpress® (Vector NTI Suite®, Invitrogen). Four different clones spanned the ORFs of *Itpr2* and *Itpr3*. To assess the tissue distribution and developmental expression of IP_3R subtypes, cDNA samples were screened with the following RT–PCR primer pairs and PCR conditions. *Itpr2*: 5′-GTGGGCTCGAAAGAGACAAG -3′ and 5′-AGACAGCTGCTTGACCAGACTCAT-3′; 95 °C for 1 min, followed by 33 cycles of 95 °C for 20 s, 55 °C for 25 s and 68 °C for 30 s. *Itpr3*: 5′-CACATTGCAATCCCAGTAACCCAGGAACTTATC-3′, 5′-ATGGGAAAAAGGCATGGATTCACTGACTAC-3′; 95 °C for 1 min, followed by 33 cycles of 95 °C for 20 s, 60 °C for 28 s and 72 °C for 40 s, then a 2 min extension at 72 °C. *Xbra* (*Xenopus* brachyury): 5′-GGATCGTTATCACCTCTG-3′, 5′-GTGTAGTCTGTAGCAGCA-3′; 95 °C for 1 min, followed by 33 cycles of 95 °C for 20 s, 55 °C for 20 s and 72 °C for 25 s. *ODC* (ornithine decarboxylase): 5′-GTCAATGATGGAGTGTATGGATC-3′, 5′-TCCATTCCGCTCTCCTGAGCAC-3′; 28 cycles of 95 °C at 20 s, 55 °C at 20 s and 72 °C at 25 s. Primers for each *Itpr* subtype spanned at least one intron in their respective genes as a control against template contamination with genomic DNA. Specificity of *Itpr* primers was confirmed by screening against *Xt-Itpr* subtype-specific clones.

Bioinformatics

Genomic organization of *Xt-Itpr* genes was inferred from the Ensembl representations (release 41, Oct 2006) of the JGI sequence data (assembly 4.1), and represented using Artemis Release 5.0 (Sanger Centre, Hinxton, U.K.). For each *Itpr* subtype, the UTR (untranslated region) sequence was confirmed using the *X. tropicalis* EST (expressed sequence tag) database (Sanger Centre).

Western blotting

For immunoblotting, samples were prepared from *Xenopus* embryos, liver and heart [10] and a *Xenopus* A6 (kidney) cell line (ATCC #CCL-102, Manassas, VA, U.S.A.). To prepare microsomes, tissues were homogenized in 50 mM Tris/HCl, 250 mM sucrose and Complete™ protease inhibitor tablet (Roche), pH 7.25, and centrifuged at 4500 ***g*** for 15 min to yield a supernatant, which was subsequently spun at 142 000 ***g*** for 35 min to yield the microsomal pellet (resuspended in 50 mM Tris/HCl and 1 mM EDTA, pH 8.3). Electrophoresis and Western blot analysis were performed using the Invitrogen NuPage™ large protein analysis system. Nitrocellulose membranes were blocked with 12 % (w/v) non-fat dried milk (Flavorite) and 1 % (w/v) BSA and subsequently probed with antibodies raised against mammalian IP_3R2 (Santa Cruz Biotechnology sc-7278) and IP_3R3 (BD Transduction Laboratories #610312). Signals were visualized using secondary antibodies coupled to horseradish peroxidase in combination with an enhanced chemiluminescence system (Pierce).

$^{45}Ca^{2+}$ efflux

X. laevis embryos, at the desired developmental stage, were homogenized in buffer (pH 7.25) containing 50 mM Tris/HCl, 250 mM sucrose and a Complete™ protease inhibitor tablet. The resulting homogenate was centrifuged at 4500 ***g*** for 15 min to yield a supernatant which was then centrifuged at 142 000 ***g*** for 35 min to yield a microsomal pellet that was resuspended in a minimal volume of the same buffer and immediately frozen in liquid nitrogen [10]. For $^{45}Ca^{2+}$ uptake, microsomes were diluted into a cytoplasmic-like buffer (20 mM Pipes, 140 mM KCl, 20 mM NaCl, 2 mM $MgCl_2$, 1 mM EGTA and 300 μM $CaCl_2$ supplemented with 7mM ATP and 30 μCi/ml of $^{45}Ca^{2+}$ at pH 7.0) for 20 min at room temperature (21 °C). After loading, microsomes were diluted into non-supplemented cytoplasmic-like buffer containing the indicated concentration of IP_3 for 3 min before filtering and rinsing on a GF/B filter. Residual radioactivity was estimated by scintillation counting (LS6500, Beckman).

RESULTS AND DISCUSSION

Xenopus IP_3R2 and IP_3R3

Xenopus tropicalis scaffolds (see Supplementary Tables 1 and 2 at http://www.BiochemJ.org/bj/404/bj4040383add.htm) containing a putative IP_3R sequence were identified through BLAST searches of genomic sequence databases using sequence from the three human IP_3R subtypes. The resulting genomic 'hits' directed the design of PCR primers used for screening cDNA derived from *X. tropicalis* ovarian tissue. Iterative sequencing of clones and subsequent PCR analyses (Supplementary Table 3) yielded full-length sequences for *Xt-Itpr2* and *Xt-Itpr3*, which correspond to mature polypeptides of 2706 and 2673 amino acids respectively. Figure 1 shows an amino acid sequence alignment of all three *X. tropicalis* IP_3R isoforms, comparing the *in vivo* sequence information for type 2 and type 3 IP_3Rs with an *in silico* predicted *X. tropicalis* IP_3R1 (2693 amino acids), based on previous data from IP_3R1 cloned from *X. laevis* [3]. The three *X. tropicalis* polypeptides have predicted molecular masses of ~306–308 kDa and display 60–70 % overall identity, with > 80 % identity with the equivalent mammalian IP_3R subtype (Table 1). Owing to this high identity, many consensus sites for protein binding and IP_3R regulation that have been characterized in mammalian IP_3R subtypes are preserved in sequence in their *Xenopus* counterparts (Figure 1).

Genomic organization of the *Xenopus Itpr* gene family

By comparing sequence from PCR-derived clones with the *X. tropicalis* genomic assembly, we were able to infer the genomic architecture of the three *Itpr* genes (Figure 2), as well as fill in missing sequence and to correct misannotations in the current *X. tropicalis* release (Supplementary Tables 1 and 2). All three *Itpr* isoforms have a highly similar genomic architecture in terms of conservation of exon number and exon length: the marked variation in genomic spans (Figure 2A) results from divergent intronic lengths (Figure 2B). A similar range of genomic spans is observed with mammalian *Itpr* isoforms (for example, ~7-fold in humans), although *Itpr3* is the most condensed *Itpr* gene (~75 kb) in the human genome and *Itpr2* possesses the broadest chromosomal span (~495 kb). Since the *Xenopus*

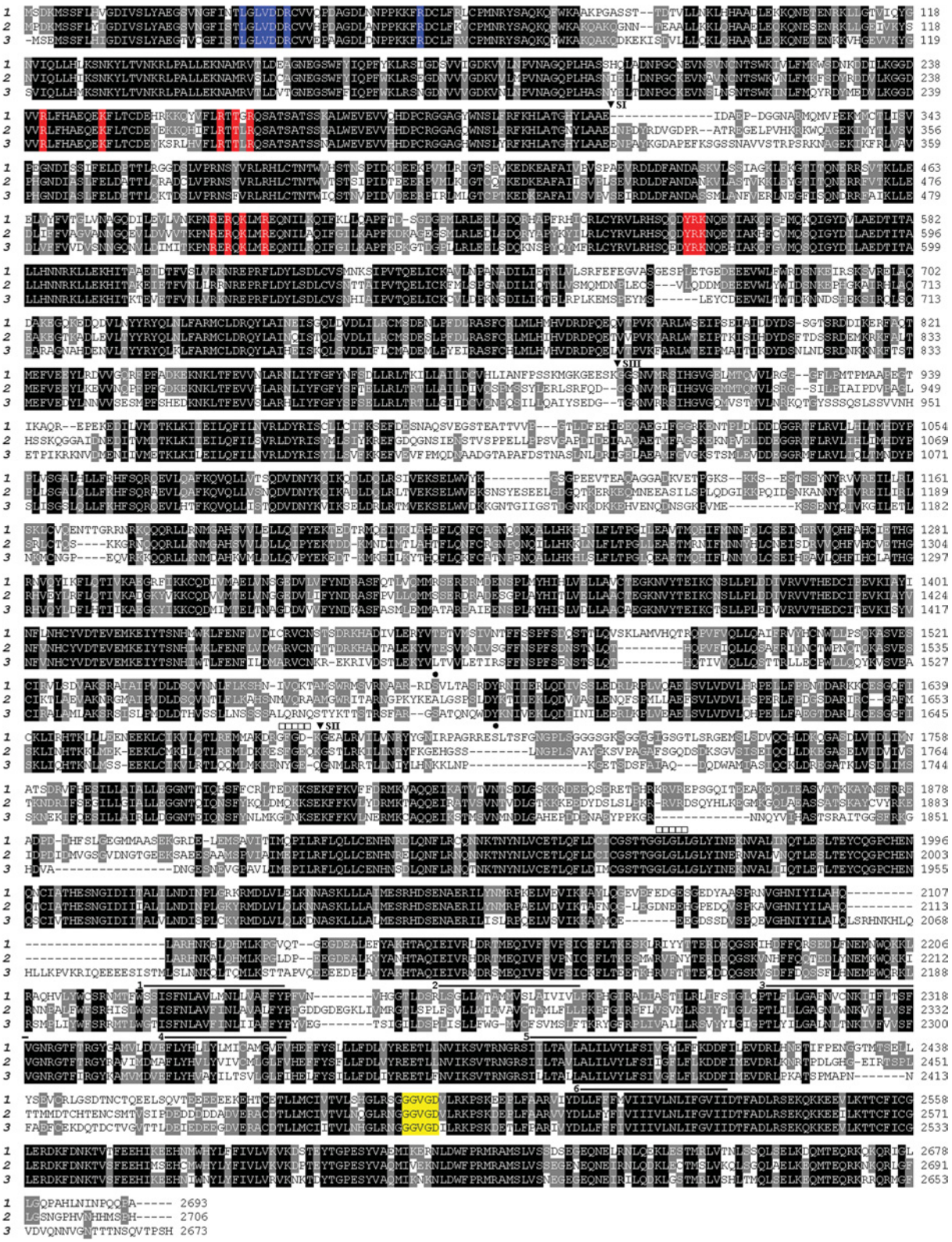

Figure 1 Sequence alignments of *Xenopus tropicalis* IP_3R isoforms

Amino acid sequence alignments of *Xt*-IP_3R1 ('1'), *Xt*-IP_3R2 ('2') and *Xt*-IP_3R3 ('3', amino acids numbered at the right), produced using the BLOSUM62 scoring matrix (ClustalW MSA). The sequence of *Xt*-IP_3R1 was predicted *in silico* with regions showing high sequence dissimilarity to the cloned *X. laevis* IP_3R1 [3] re-evaluated by sequencing cDNA from *X. tropicalis* oocytes. Identical amino acids conserved across all three *Xenopus* isoforms are highlighted in black, residues conserved in any two polypeptides are shaded grey. Specific residues that are important for IP_3R function are highlighted and include IP_3-co-ordinating residues within the binding core (residues 224–589 of *Xt*-IP_3R1, red), residues predicted to suppress IP_3-binding affinity within the suppressor domain (residues 1–223 of *Xt*-IP_3R1, blue) and C-terminal residues between transmembrane regions 5 and 6 (yellow) that comprise the channel selectivity filter [13]. Predicted transmembrane domains (solid lines, numbered), mammalian IP_3R1 splice site locations (▼) and consensus sites for PKA (protein kinase A) phosphorylation (IP_3R1, ●) and ATP binding (IP_3R1, □) are also shown.

Table 1 Amino acid sequence identities between *X. tropicalis* and mammalian IP_3R isoforms

Full-length polypeptides were aligned using the BLOSUM62 scoring matrix (ClustalW MSA). The following accession numbers were used for mammalian subtype sequence [*Homo sapiens* (Hs): IP_3R1, Q14643; IP_3R2, Q14571; IP_3R3, Q14573; *Rattus norvegicus* (Rn): IP_3R1, P29994; IP_3R2, P29995; IP_3R3, Q63269]. The *in silico* predicted *X. tropicalis* IP_3R1 displays 98 % amino acid identity with the *X. laevis* IP_3R1 isolated from an oocyte cDNA library ([3], D14400).

	Xt IP_3R2	*Xt* IP_3R3	*Hs* IP_3R1	*Rn* IP_3R1	*Hs* IP_3R2	*Rn* IP_3R2	*Hs* IP_3R3	*Rn* IP_3R3
Xt IP_3R1	68	60	**89**	**88**	68	68	60	60
Xt IP_3R2		62	68	67	**88**	**88**	63	62
Xt IP_3R3			60	59	62	62	**82**	**82**

genomic sequence is currently a scaffold-based (rather than chromosomal) assembly, the estimation of intronic lengths contains approximations, especially where genes span different scaffolds (Supplementary Tables 1 and 2) and where the intervening sequence is incomplete. For all scaffold-breaks, RT–PCR analysis was performed to confirm that primers localized in different genomic scaffolds could amplify a contiguous transcript. Additionally, neighbouring genes of *Xt-Itpr1* (e.g. *sumf1-Itpr1-BHLHB2*), *Xt-Itpr2* (e.g. *NYSAR95-Itpr2-SSPN*) and *Xt-Itpr3* (e.g. *BAK1-Itpr3-GRM4*) are syntenous with human *Itpr* loci, supporting the predicted organization. All of the *Xenopus* predicted exon–intron boundaries conformed to the GT/AG rule for splice donor and acceptor sites.

Sequential mapping of exon size along the sequence of each *Itpr* isoform underscored the overall similarity in genetic architecture (Figure 2C), but also highlighted individual features of the three

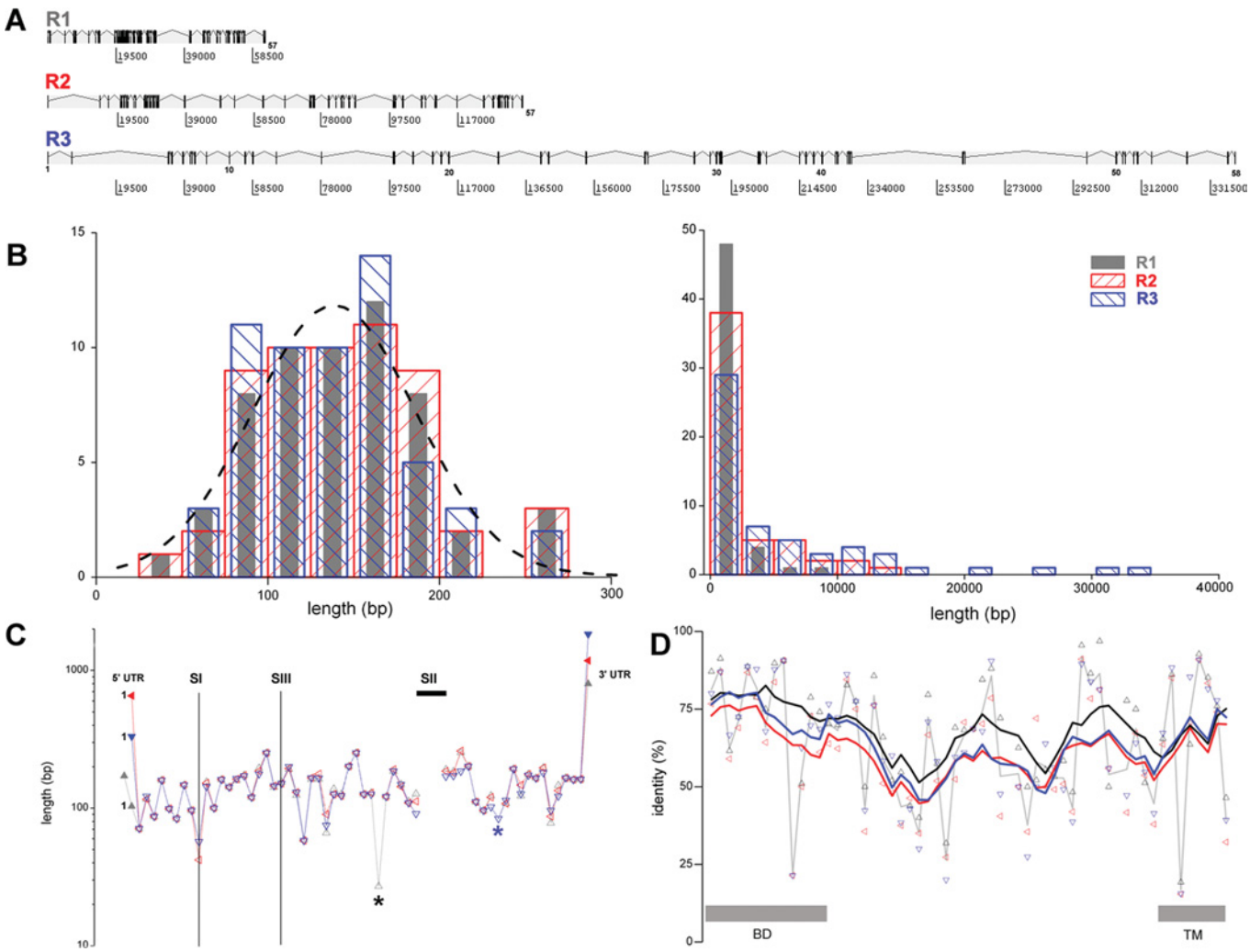

Figure 2 Genomic architecture of the *Itpr* gene family

(**A**) Schematic representation of genomic organization of *Xt-Itpr* subtypes. Exons (numbered) are depicted as vertical bars with appropriate spacing on a basepair scale (below). (**B**) Cumulative distribution of exon (left) and intron (right) lengths for *Xt*-IP_3R1 (grey), *Xt*-IP_3R2 (red) and *Xt*-IP_3R3 (blue). The distributions are derived only from exons composed entirely of protein-coding sequence, i.e. excluding exons that comprise the 5′- and 3′-UTR. The broken line is a Gaussian fit to the entire dataset (mean = 140 bp). (**C**) Conservation of exon length of *Itpr* genes. The length (logarithmic *y*-axis) of successive exons, numbered from the first exon containing ORF, in *Xt-Itpr1* (black triangle), *Xt-Itpr2* (red triangle) and *Xt-Itpr3* (blue triangle) is plotted sequentially along the *x*-axis to facilitate comparison of the coding architecture of each isoform. Locations of unique exons (asterisks) and splice sites (SI, SII and SIII) identified in mammalian *Itpr1* genes (lines) are highlighted. Exons containing UTRs are shown by solid symbols. SI, SII and the usage of an alternative exon splice site for SIII are absent from *Xt-Itpr1*. (**D**) Amino acid identity, analysed at an exon-by-exon level, between *Xt-Itpr1* and *Xt-Itpr2* (black triangle), *Xt-Itpr1* and *Xt-Itpr3* (red) and *Xt-Itpr2* and *Xt-Itpr3* (blue) scored using BLOSUM45. Average point-to-point values (thin grey line) and rolling six exon averages of raw identity scores (coloured lines) are connected. Regions of the polypeptide designated as the binding domain (BD) and the C-terminal transmembrane domain (TM) are shown.

Table 2 Organization of *Xenopus Itpr* genes

Genomic architecture of *X. tropicalis Itpr* genes derived from datasets depicted in Figure 2. Data for exons containing UTRs, which may be partial, are excluded from the averages. Only exon sizes are known exactly because of regions of missing intronic sequence ('*N*'s) within the available genomic dataset.

	Xt-Itpr1	*Xt-Itpr2*	*Xt-Itpr3*
Protein-coding exons	57	57	58
Average exon (bp)	141.8	142.4	138.3
Average intron (bp)	~990	~2400	~5900
Genomic span (kb)	~62	~20	~340
5′-UTR (bp)	~187	~562	~265
3′-UTR (bp)	~715	~1094	~1734

Xenopus Itpr isoforms. First, unique exons are present in *Xt-Itpr1* and *Xt-Itpr3* (exon 33 in type 1, exon 46 in type 3, asterisked in Figure 2C). The unique type 3 exon, which encodes sequence preceding the channel domain of the *Itpr*, is also found in human type 3 *Itpr*. The short type 1 unique exon (27 bp), within the modulatory domain of *Xt-Itpr1*, is absent from mammalian *Itpr* type 1 sequences. Secondly, in terms of splice variants, ovarian transcripts of *Xt-Itpr1* did not contain sequences corresponding to alternatively spliced insertions found in mammalian *Itpr1* transcripts (SI, SII and SIII [15]), i.e. the ovarian transcript is $SI^{-}SII^{-}SIII^{-}$ [3]. The type 2 and type 3 *Xt-Itpr* isoforms possess exonic sequence of equivalent length to the missing SI in *Itpr1* cDNA, such that the total number of exons containing translated sequence is 57 for *Itpr1*, 57 for *Itpr2* and 58 for *Itpr3* (owing to the additional unique exon).

With the exception of the 5′-UTR for *Xt-Itpr1*, which was split by a large intron (> 30000 bp, cf. < 1000 bp for average ORF intron size), the 5′- and 3′-UTRs for each *Itpr* subtype were all encoded within single exons containing the ORF (Figure 2C, Table 2). The 5′-UTRs for *Xt-Itpr1* and *Xt-Itpr2* lacked upstream AUG codons, whereas the 5′-UTR for *Xt-Itpr3* contained a potential upstream ORF (−66 to −39 bp). However, the short length, separation and unfavourable initiation context of the upstream AUG probably does not prevent translation at the distal AUG [28,29]. For each subtype, the translation-initiation codon was immediately preceded by sequence conforming well to the optimized consensus described for vertebrates (GCCRCC-[ATG]G [29]). The predicted 3′-UTR sequences, probably crucial for developmental regulation of mRNA translation/stability, were longer than the respective 5′-UTRs (Table 2, Figure 2C), and all 3′-UTRs contained a consensus polyadenylation signal (AAUAAA) 15–20 bp upstream of the poly(A) tail. The average length of the predicted 5′- and 3′-UTR for the *Itpr* genes was greater than reported 'average' values for the *Xenopus* dataset (5′-UTR, ~150 bp; 3′-UTR, ~500 bp [30]). Finally, a plot of exon-by-exon homology between the three subtypes (Figure 2D) showed that, at the exon level, regions of high sequence identity were distributed throughout the entire primary sequence and not solely confined to the N-terminal IP_3-binding and C-terminal transmembrane domains. Greater identity was observed between individual exons of *Xt-Itpr1* and *Xt-Itpr2* for the majority of exons (~55 % of total, 35/56 analysed) than *Xt-Itpr2* to *Xt-Itpr3* (~35 %) or *Xt-Itpr1* to *Xt-Itpr3* (~10 %). This relationship, which potentially implies evolutionary pedigree, is clearly manifest in the rolling averages (six exon window) of these datasets (Figure 2D).

Distribution of *Xenopus Itpr2* and *Itpr3* mRNA

First, we examined the developmental expression of *Itpr2* and *Itpr3* mRNA in staged *X. laevis* embryos using semi-quantitative RT–PCR (Figure 3A). In unfertilized eggs and early embryonic stages preceding the MBT (mid-blastula transition), maternally inherited *Itpr3* mRNA was not detected. In contrast, *Itpr2* mRNA was present in unfertilized *X. laevis* eggs and early cleavage stages in all donors examined ($n = 4$). Transcripts for both IP_3R subtypes, however, were easily detectable by late gastrulation (stage 12), and mRNA levels were subsequently maintained throughout embryogenesis (tested up to ~2 days post-fertilization). These data are consistent with initiation of transcription of the zygotic genome starting during MBT, consistent with *Xbra* controls. Transcripts for *Itpr1* were inherited maternally and persisted throughout embryogenesis, as discussed previously [31]. The early embryonic presence of *Itpr2* mRNA was investigated further by RT–PCR in whole ovarian tissue as well as in stage VI oocytes from both *X. laevis* and *X. tropicalis* (Figure 3B). Consistent with results in *X. laevis* eggs, *Itpr2* mRNA was detectable in *X. laevis* stage VI oocytes ($n = 4$ donors), but especially in whole ovarian tissue samples. The possibility of contamination of the stage VI oocytes cDNA signal from residual follicular tissue mRNA is unlikely, owing to careful preparation of the oocytes, as well as the results from eggs (Figure 3A) which have been shed from the frog. *Itpr2* mRNA was also evident in similarly sourced samples from *X. tropicalis* (Figure 3B). For *Itpr3* mRNA, signals were weak in *X. laevis* oocytes (positive in only one from four donors), again consistent with data from *X. laevis* eggs (Figure 3A). *Itpr3* mRNA was, however, consistently detected in *X. laevis* ovarian tissue samples (Figure 3B; $n = 4$ donors). However, in *X. tropicalis*, *Itpr3* mRNA was seen in both oocytes and, especially, ovarian tissue samples, in all donor frogs examined ($n = 4$). Therefore, despite the close similarity between these species of pipid frogs, there was unexpected variation in the presence of transcripts of different IP_3R subtypes. These differences could reflect a physiological adaptation to the different ambient temperatures at which these species thrive (16–20 °C compared with 24–25 °C), and contribute to differences observed in physiological studies with *X. tropicalis* [27].

Using commercial antibodies with the highest available epitope identity (> 90 %) with the sequence of *Xenopus* IP_3R2 and IP_3R3 subtypes, we observed immunoreactive bands in samples from pre-tailbud stage (stage 25) embryos (Figure 3C). For IP_3R3, a band was observed at ~235 kDa in both stage 25 embryos and A6 cell line samples, a cell line derived from kidney epithelium which is enriched in *Itpr3* mRNA (results not shown). This value represents a lower molecular mass than for *X. laevis* IP_3R1 (250–255 kDa [3,10]) and is consistent with values reported for mammalian IP_3R3 (222–250 kDa [32,33]). For anti-IP_3R2 antibodies, a band was observed (~270 kDa) in both stage 25 embryos (Figure 3C), as well as adult frog heart and liver samples, tissues which express *Itpr2* in mammals [14]. The higher molecular mass of IP_3R2 (*Xt*-IP_3R2 is 33 amino acids longer than *Xt*-IP_3R3) is consistent with other data for IP_3R2 (260 kDa [34]), although the possibility of cross-reactivity with currently available commercial antibodies cannot be excluded at present.

Finally, to assess the sensitivity of intracellular Ca^{2+} stores to IP_3 at developmental stages which show changes in expression of *Itpr2* and *Itpr3* mRNA, we prepared microsomes from stage 8 and stage 25 embryos, namely before and significantly after (~24 h) transcriptional activation of the zygotic genome. A submaximal concentration of IP_3 (100 nM) releases a greater proportion of the IP_3-sensitive Ca^{2+} store in stage 25 compared with stage 8 embryos (47.6 ± 1.7 % compared with 25.9 ± 2.6 %; $n \geqslant 3$ independent donor frogs), indicative of an increased *in vivo* sensitivity to IP_3. In parallel, the observed size of the IP_3-sensitive Ca^{2+} store decreased (Figure 3D), although a caveat is that this parameter is likely to be sensitive to the changing cellular

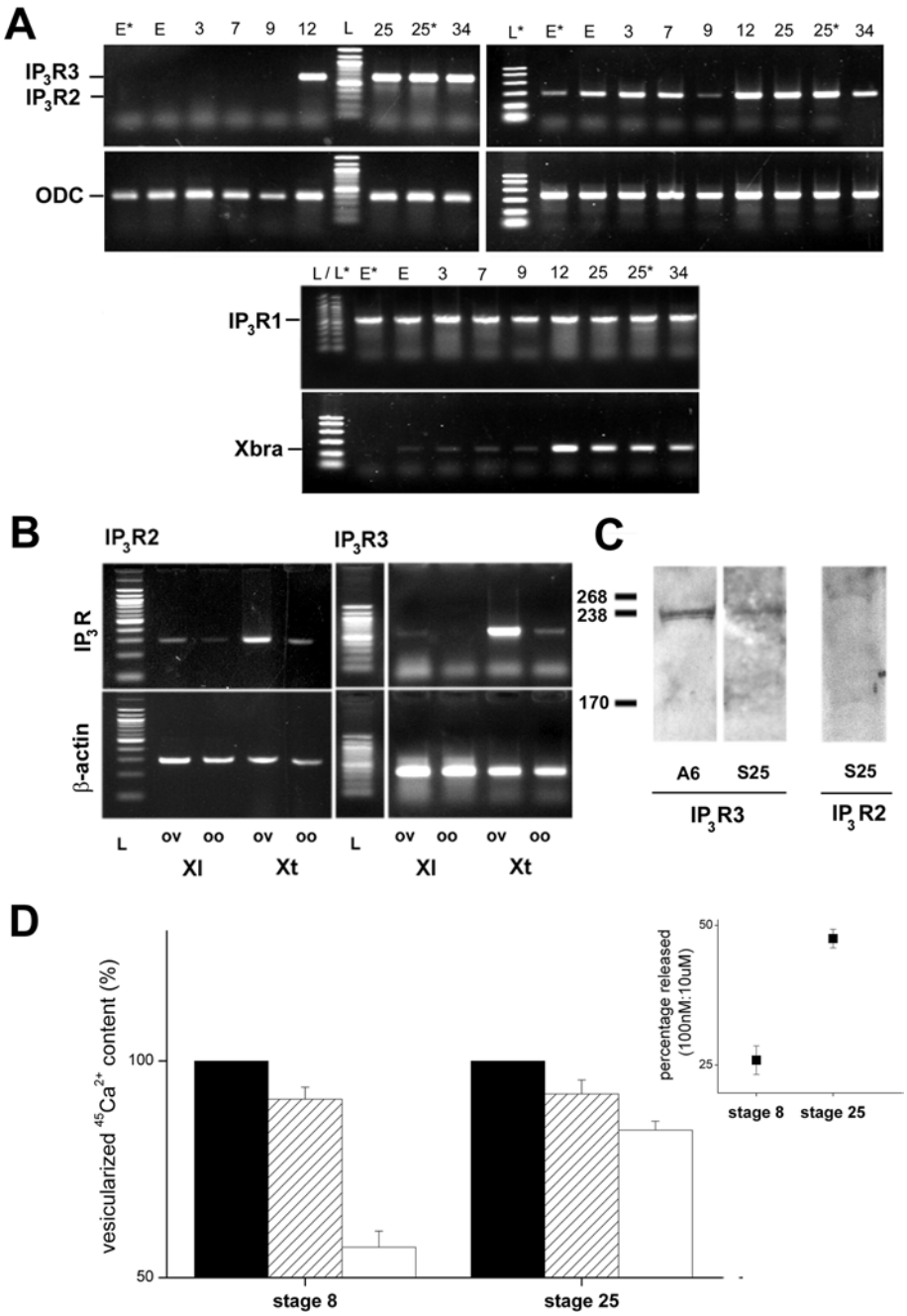

Figure 3 Expression of *Xenopus Itpr* subtypes

(**A**) Developmental expression of *Itpr1* (middle), *Itpr2* (right) and *Itpr3* (left) mRNA analysed by RT–PCR. mRNA was extracted from eggs (E and E*, different donor samples) and a variety of developmental stages [3, 7, 9, 12, 25, 25* (different donor sample) and 34]. Specificity of amplification from stage-specific cDNA was confirmed by sizing (L, 100 bp ladder N3231S, NEB; L*, PCR marker ladder #G3161, Promega) and sequencing. Reactions for ODC as a loading control (expected product size of 385 bp) and Xbra (expected product size of 187bp) are shown. (**B**) RT–PCR screening of *Itpr2* and *Itpr3* mRNA in ovarian tissue ('ov') and stage VI oocytes ('oo') in *X. laevis* ('Xl') and *X. tropicalis* ('Xt'). Upper panels, *Itpr2* and *Itpr3* diagnostic primers. Lower panels, loading controls were either β-actin (*Itpr2*, left) or ODC (*Itpr3*, right). (**C**) Immunological identification of IP_3R2 and IP_3R_3. Lanes were loaded with 30 μg of protein from either the *Xenopus* A6 kidney cell line (A6) or stage 25 embryos (S25) and probed with anti-IP_3R3 or anti-IP_3R2. Molecular-mass marker sizes are indicated in kDa. (**D**) $^{45}Ca^{2+}$ efflux analysis of microsomes prepared from pre-MBT (stage 8, left) and tailbud-stage embryos (stage 25, right), showing the proportion of the total $^{45}Ca^{2+}$ content (closed bars) released by submaximal (100 nM, hatched bars) and maximal concentrations of IP_3 (10 μM, open bars). Data were compared only from embryos prepared from the same donor animal ($n \geqslant 3$ independent donors). Inset, proportion of IP_3-sensitive Ca^{2+} store mobilized by 100 nM IP_3 as a percentage of the response to 10 μM IP_3 as a crude index of sensitivity.

specialization of the developing embryos. Nevertheless, an increased global sensitivity to IP_3 and a decreased store size are both adaptations that have been observed to result from an increased expression of IP_3Rs [35].

Evolution of IP_3R subtypes

In conjunction with the data of Kume et al. [3], the biologically verified (cf. annotated) sequence of all three *Xenopus* IP_3Rs

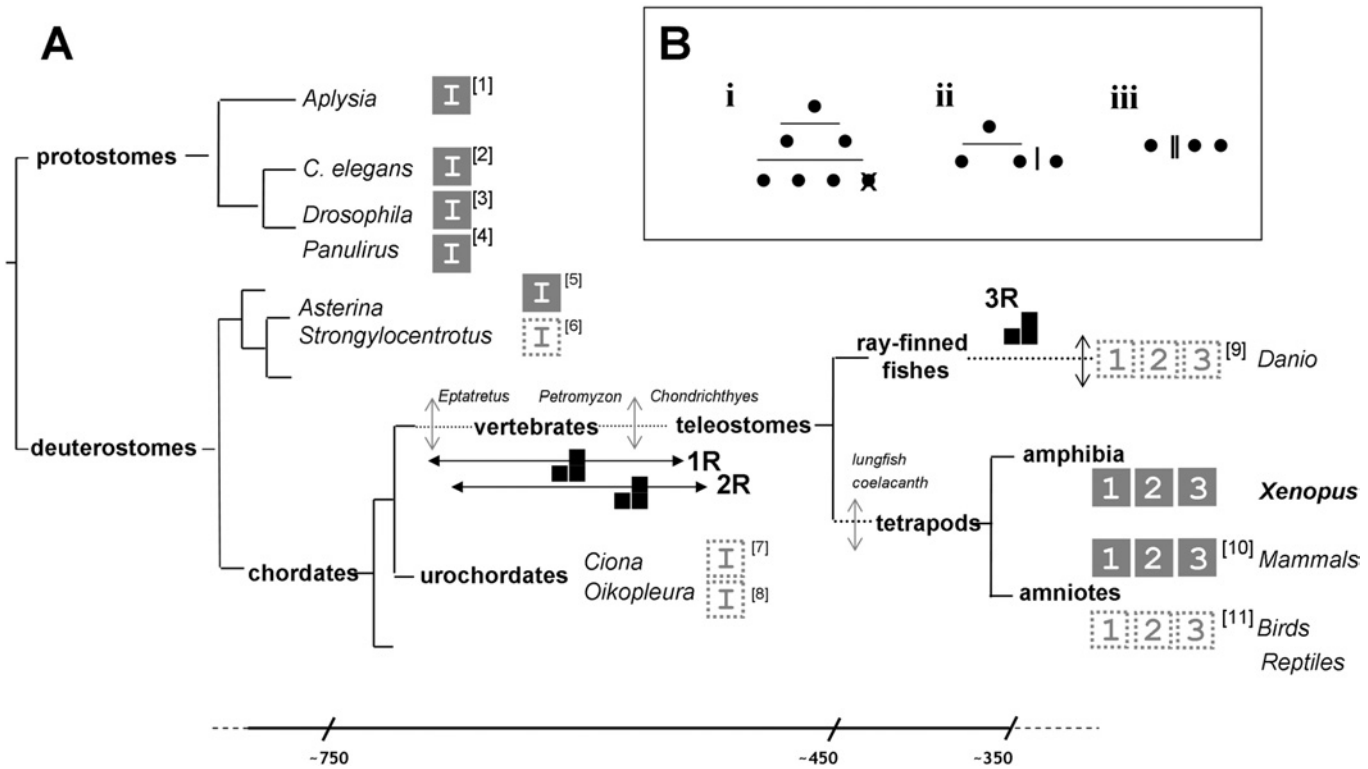

Figure 4 Molecular evolution of the *Itpr* gene family

(**A**) A simplified triploblast phylogeny, drawn on the basis of the Protostomia (Lophotrochozoa–Ecdysozoa)–Deuterostomia classification to highlight the evolutionary diversification of the *Itpr* gene family. For clarity, certain nodes have been omitted and are represented by a broken line with a vertical arrow to indicate intermediate divergence of lineages. Approximate timings (millions of years) are shown on a non-linear scale (bottom). Proposed timings of WGD events (1R, 2R and 3R) are indicated on the appropriate branch of the phylogeny. Key model organisms (italicized), including those in which a single *Itpr* gene ('I') or multiple *Itpr* genes (subtype '1', '2' and '3') have been confirmed by sequencing of a full-length clone from biological material (solid box), or predicted in part by genome annotation (dashed box) are shown. Accession numbers (square brackets) are as follows: '1', DQ397517 (*Aplysia californica*); '2', AJ243181 (*Caenorhabditis elegans*); '3', D90403 (*Drosophila melanogaster*); '4', AF055079 (*Panilurus argus*); '5', AB071372 (*Asterina pectinifera*) [38]; '6', XR_025864 (*Strongylocentrotus purpuratus*) '7', ENSCING00000007322 (*Ciona intestinalis*) and ENSCSAVG00000006185 (*Ciona savignyi*); '8', AAT47836 (*Oikopleura dioica*); '9', XM_685965 and XP_693046 (*Danio rerio*); '11', XM_414438, XM_001235612 and XM_418035 (*Gallus gallus*) [36]. For mammalian IP_3R diversity ('10'), see [14,16]. (**B**) Alternative gene duplication pedigrees leading to three *Itpr* paralogues are represented by (i) two WGD (2R, horizontal lines), followed by gene loss, (ii) one round of WGD (1R) followed by a more localized duplication (vertical line), or (iii) two successive local duplications.

represents the first report of full-length sequence for all three IP_3R subtypes outside the mammalian lineage, where the properties of each of the three members of this gene family have been extensively investigated [12–14]. Therefore, in terms of evolutionary diversification of IP_3R subtypes, we speculate on two questions: first, at what evolutionary timepoint are discrete *Itpr* genes first identifiable, and, secondly, what genetic mechanisms (small-scale or large-scale duplication events with subsequent gene loss) underpinned the generation of IP_3R diversity in the vertebrate lineage?

First, when did *Itpr* duplication first occur? Combining our knowledge of (i) the three *Itpr* genes in mammals [12–14] and birds (from genetic ablation studies in DT40 cells [36]) with (ii) our identification of three *Itpr* genes in a non-amniote lineage suggests that IP_3R subtype radiation occurred before the emergence of a common tetrapod ancestor. Furthermore, since three IP_3R subtypes have recently been validated from zebrafish [36a], the most parsimonious explanation is that IP_3R isoform radiation had occurred before the emergence of the common teleostome ancestor, rather than via multiple independent duplications in each separate chordate lineage (but see [37]). Analysis of more primitive deuterostomes (best exemplified in echinoderms through cloning of a single starfish IP_3R [38], as well as urochordate genomic annotations), provides evidence for only a single IP_3R isoform (Figure 4). Therefore the ancestral deuterostome lineage possessed a sole *Itpr* gene, delimiting the *Itpr* duplication events to the period between the base of the chordate clade (post-divergence of the vertebrate and urochordates) and the expansion of the bony vertebrates ($\sim$750 to $\sim$450 million years ago). Refinement of this estimate will be possible by analysis of chordates spanning key intermediate nodes, such as the jawless vertebrates *Eptatretus* (hagfish), *Petromyzon* (lamprey) and cartilaginous fish, several of which are currently the focus of whole-genome sequencing efforts. Notably, the lack of currently available data reporting multiple *Itpr* genes in basal deuterostomes and protostomes (Figure 4), as well as 'simpler' eukaryotes [39,40], does not necessarily imply lower functional complexity. The extent of alternative splicing in duplicated genes is lower than in singletons [41], and a prevalence of alternatively spliced IP_3R variants in protostomes could represent an alternate strategy for customizing the role of IP_3R subtypes in cellular Ca^{2+} signalling.

Secondly, mechanistically, the scope of the genome rearrangements underpinning duplication events has long been the subject of controversial debate, with evidence for massive early WGD (whole-genome duplication) event(s), a maintained rate of more localized (single gene or segmental) 'continuous duplications', or a combination of both [37,42–44]. The timeframe during which multiple *Itpr* genes emerged (Figure 4) corresponds with the timings of two rounds (1R/2R) of WGD events proposed in early

vertebrate evolution (the '2R hypothesis' [42,43,45]), when the majority of tetrapod gene family duplicates arose [45]. The low duplication retention rate within the *X. tropicalis* lineage [45] and the presence of three coding *Itpr* genes in different tetrapod lineages support further the idea of two early duplication events occurring via either two WGDs (producing four *Itpr* paralogues followed by gene loss) or a single WGD followed by a more localized duplication, rather than two more localized duplications in multiple lineages (Figure 4B). A more global synteneic analysis (difficult because the current *Xenopus* assembly is scaffold-based) and more extensive (in terms of outgroups) study would be needed to discriminate between these options. Additional studies of IP_3R diversity in the actinopterygian lineage (ray-finned fishes) would also be welcome, owing to the additional fish-specific genome duplication event ('3R' [46]) and the high retention rates of duplicates in certain teleosts (e.g. zebrafish [45]). This is because diminution of *Itpr* gene diversity from a polyploidy background down to only three functional genes, just like tetrapods, would provide new impetus for understanding the specific purpose of three discrete IP_3R subtypes in cellular physiology.

Work in the laboratory is supported by the NIH (National Institutes of Health) (NS046783) and a NSF (National Science Foundation) CAREER Fellowship Award (to J. S. M.).

REFERENCES

1 Parker, I. and Yao, Y. (1991) Regenerative release of calcium from functionally discrete subcellular stores by inositol trisphosphate. Proc. R. Soc. London Ser. B **246**, 269–274

2 Lechleiter, J. D., Girard, S., Peralta, E. and Clapham, D. (1991) Spiral calcium wave propagation and annihilation in *Xenopus laevis* oocytes. Science **252**, 123–126

3 Kume, S., Muto, A., Aruga, J., Nakagawa, T., Michikawa, T., Furuichi, T., Nakade, S., Okano, H. and Mikoshiba, K. (1993) The *Xenopus* IP_3 receptor: structure, function and localization in oocytes and eggs. Cell **73**, 555–570

4 Kume, S., Yamamoto, A., Inoue, T., Muto, A., Okano, H. and Mikoshiba, K. (1997) Developmental expression of the inositol 1,4,5-trisphosphate receptor and structural changes in the endoplasmic reticulum during oogenesis and meiotic maturation of *Xenopus laevis*. Dev. Biol. **182**, 228–239

5 Terasaki, M., Runft, L. L. and Hand, A. R. (2001) Changes in organization of the endoplasmic reticulum during *Xenopus* oocyte maturation and activation. Mol. Biol. Cell **12**, 1103–1116

6 Machaca, K. (2004) Increased sensitivity and clustering of elementary Ca^{2+} release events during oocyte maturation. Dev. Biol. **275**, 170–182

7 Boulware, M. J. and Marchant, J. S. (2005) IP_3 receptor activity is differentially regulated in endoplasmic reticulum subdomains during oocyte maturation. Curr. Biol. **15**, 765–770

8 Muto, A., Kume, S., Inoue, T., Okano, H. and Mikoshiba, K. (1996) Calcium waves along the cleavage furrows in cleavage-stage *Xenopus* embryos and its inhibition by heparin. J. Cell Biol. **135**, 181–190

9 Kume, S., Muto, A., Inoue, T., Suga, K., Okano, H. and Mikoshiba, K. (1997) Role of the inositol 1,4,5-trisphosphate receptor in ventral signaling in *Xenopus* embryos. Science **278**, 1940–1943

10 Parys, J. B., Sernett, S. W., DeLisle, S., Snyder, P. M., Welsh, M. J. and Campbell, K. P. (1992) Isolation, characterization and localization of the inositol 1,4,5-trisphosphate receptor protein in *Xenopus laevis* oocytes. J. Biol. Chem. **267**, 18776–18782

11 Parys, J. B. and Bezprozvanny, I. (1995) The inositol trisphosphate receptor of *Xenopus* oocyte. Cell Calcium **18**, 353–363

12 Patel, S., Joseph, S. K. and Thomas, A. P. (1999) Molecular properties of inositol 1,4,5-triphosphate receptors. Cell Calcium **25**, 247–264

13 Bosanac, I., Michikawa, T., Mikoshiba, K. and Ikura, M. (2004) Structural insights into the regulatory mechanism of IP_3 receptor. Biochim. Biophys. Acta **1742**, 89–102

14 Taylor, C. W., Genazzani, A. A. and Morris, S. A. (1999) Expression of inositol trisphosphate receptors. Cell Calcium **26**, 237–251

15 Regan, M. R., Lin, D. D. M., Emerick, M. C. and Agnew, W. S. (2005) The effect of higher order RNA processes on changing patterns of protein domain selection: a developmentally regulated transcriptome of type 1 inositol 1,4,5-trisphosphate receptors. Proteins Struct. Funct. Bioinformatics **59**, 312–331

16 Iwai, M., Tateishi, Y., Hattori, M., Mizutani, A., Nakamura, T., Futatsugi, A., Inoue, T., Furuichi, T., Michikawa, T. and Mikoshiba, K. (2005) Molecular cloning of mouse type 2 and type 3 inositol 1,4,5-trisphosphate receptors and identification of a novel type 2 receptor splice variant. J. Biol. Chem. **280**, 10305–10317

17 Futatsugi, A., Kuwajima, G. and Mikoshiba, K. (1998) Muscle-specific mRNA isoform encodes a protein composed mainly of the N-terminal 175 residues of type 2 Ins(1,4,5)P_3 receptor. Biochem. J. **334**, 559–563

18 Newton, C. L., Mignery, G. A. and Südhof, T. C. (1994) Co-expression in vertebrate tissues and cell lines of multiple inositol 1,4,5-trisphosphate ($InsP_3$) receptors with distinct affinities for $InsP_3$. J. Biol. Chem. **269**, 28613–28619

19 Wojcikiewicz, R. J. H. and Luo, S. G. (1998) Differences among type I, II, and III inositol-1,4,5-trisphosphate receptors in ligand-binding affinity influence the sensitivity of calcium stores to inositol-1,4,5-trisphosphate. Mol. Pharmacol. **53**, 656–662

20 Tu, H., Wang, Z., Nosyreva, E., De Smedt, H. and Bezprozvanny, I. (2005) Functional characterization of mammalian inositol 1,4,5-trisphosphate receptor isoforms. Biophys. J. **88**, 1046–1055

21 Miyakawa, T., Maeda, A., Yamazawa, T., Hirose, K., Kurosaki, T. and Iino, M. (2000) Encoding of Ca^{2+} signals by differential expression of IP_3 receptor subtypes. EMBO J. **18**, 1303–1308

22 Hattori, M., Suzuki, A. Z., Higo, T., Miyauchi, H., Michikawa, T., Nakamoura, T., Inoue, T. and Mikoshiba, K. (2004) Distinct roles of inositol 1,4,5-trisphosphate receptor types 1 and 3 in Ca^{2+} signaling. J. Biol. Chem. **279**, 11967–11975

23 Danoff, S. K., Ferris, C. D., Donath, C., Fischer, G. A., Munemitsu, S., Ullrich, A., Snyder, S. H. and Ross, C. A. (1991) Inositol 1,4,5-trisphosphate receptors: distinct neuronal and non-neuronal forms derived by alternative splicing differ in phosphorylation. Proc. Natl. Acad. Sci. U.S.A. **88**, 2951–2955

24 Khan, A. A., Soloski, M. J., Sharp, A. H., Schilling, G., Sabatini, D. M., Li, S.-H., Ross, C. A. and Snyder, S. H. (1996) Lymphocyte apoptosis: mediation by increased type 3 inositol 1,4,5-trisphosphate receptor. Science **273**, 503–507

25 Mendes, C. C., Gomes, D. A., Thompson, M., Souto, N. C., Goes, T. S., Goes, A. M., Rodriques, M. A., Gomez, M. V., Nathanson, M. H. and Leite, M. F. (2005) The type III inositol 1,4,5-trisphosphate receptor preferentially transmits apoptotic Ca^{2+} signals into mitochondria. J. Biol. Chem. **280**, 40892–900

26 Futatsugi, A., Nakamura, T., Yamada, M. K., Ebisui, E., Nakamura, K., Uchida, K., Kitaguchi, T., Takahashi-Iwanaga, H., Noda, T., Aruga, J. and Mikoshiba, K. (2005) IP_3 receptor types 2 and 3 mediate exocrine secretion underlying energy metabolism. Science **309**, 2232–2234

27 Marchant, J. S. and Parker, I. (2001) *Xenopus tropicalis* oocytes as an advantageous model system for the study of intracellular Ca^{2+} signaling. Br. J. Pharmacol. **132**, 1396–1410

28 Luukkonen, B. G. M., Tan, W. and Schwartz, S. (1995) Efficiency of reinititaion of translation on human immunodeficiency virus type 1 mRNAs is determined by the length of the upstream open reading frame and by intercistronic distance. J. Virol. **69**, 4086–4094

29 Kozak, M. (1987) An analysis of 5′-noncoding sequences from 699 vertebrate messenger RNAs. Nucleic Acids Res. **15**, 8125–8143

30 van der Velden, A. W., Los, A., Voorma, H. O. and Thomas, A. A. M. (2000) Sequence and translation initiation properties of the *Xenopus* TGFβ5, PDGF-A, and PDGF-α receptor 5′ untranslated regions. Int. J. Dev. Biol. **44**, 851–859

31 Kume, S., Muto, A., Okano, H. and Mikoshiba, K. (1997) Developmental expression of the inositol 1,4,5-trisphosphate receptor and localization of inositol 1,4,5-trisphosphate during early embryogenesis in *Xenopus laevis*. Mech. Dev. **66**, 157–168

32 Joseph, S. K., Lin, C., Pierson, S., Thomas, A. P. and Maranto, A. R. (1995) Heteroligomers of type-I and type-III inositol trisphosphate receptors in WB rat liver epithelial cells. J. Biol. Chem. **270**, 23310–23315

33 Cardy, T. J. A., Traynor, D. and Taylor, C. W. (1997) Differential regulation of types-1 and -3 inositol trisphosphate receptors by cytosolic Ca^{2+}. Biochem. J. **328**, 785–793

34 Perez, P. J., Ramos-Franco, J., Fill, M. and Mignery, G. A. (1997) Identification and functional reconstitution of the type 2 inositol 1,4,5-trisphosphate receptor from ventricular cardiac myocytes. J. Biol. Chem. **272**, 23961–23969

35 Kasri, N. N., Kocks, S. L., Verbert, L., Hebert, S. S., Callewaert, G., Parys, J. B., Missiaen, L. and De Smedt, H. (2006) Up-regulation of inositol 1,4,5-trisphosphate receptor type 1 is responsible for a decreased endoplasmic-reticulum Ca^{2+} content in presenilin double knock-out cells. Cell Calcium **40**, 41–51

36 Sugawara, H., Kurosaki, M., Takata, M. and Kurosaki, T. (1997) Genetic evidence for involvement of type1, type 2 and type 3 inositol 1,4,5-trisphosphate receptors in signal transduction through the B-cell antigen receptor. EMBO J. **11**, 3078–3088

36a Ashworth, R., Devogelaere, B., Fabes, J., Tunwell, R. E., Koh, K. R., De Smedt, H. and Patel, S. (2007) Molecular and functional characterization of inositol trisphosphate receptors during early zebrafish development. J. Biol. Chem. **282**, 13984–13993

37 Hughes, A. L. and Friedman, R. (2004) Pattern of divergence of amino acid sequences encoded by paralogous genes in human and pufferfish. Mol. Phylogenet. Evol. **32**, 337–343
38 Iwasaki, H., Chiba, K., Uchiyama, T., Yoshokawa, F., Suzuki, F., Ikeda, M., Furuichi, T. and Mikoshiba, K. (2002) Molecular characterization of the starfish inositol 1,4,5-trisphosphate receptor and its role during oocyte maturation and fertilization. J. Biol. Chem. **277**, 2763–2772
39 Traynor, D., Milne, J. L. S., Insall, R. H. and Kay, R. R. (2000) Ca^{2+} signaling is not required for chemotaxis in *Dictyostelium*. EMBO J. **19**, 4864–4854
40 Ladenburger, E.-M., Korn, I., Kasielke, N., Wassmer, T. and Plattner, H. (2006) An Ins(1,4,5)P_3 receptor in *Paramecium* is associated with the osmoregulatory system. J. Cell Sci. **119**, 3705–3717.
41 Kopelman, N. M., Lancet, D. and Yanai, I. (2005) Alternative splicing and gene duplication are inversely correlated evolutionary mechanisms. Nat. Genet. **37**, 588–589
42 Ohno, S. (1970) Evolution by gene duplication, Springer-Verlag, New York
43 Dehal, P. and Boore, J. L. (2005) Two rounds of whole genome duplication in the ancestral vertebrate. PLoS Biol. **3**, 1700–1708
44 Gu, X., Wang, Y. and Gu, J. (2002) Age distribution of human gene families shows significant roles of both large- and small-scale duplications in vertebrate evolution. Nat. Genet. **31**, 205–208
45 Blomme, T., Vandepoele, K., De Bodt, S., Simillion, C., Maere, S. and van der Peer, Y. (2006) The gain and loss of genes during 600 million years of vertebrate evolution. Genome Biol. **7**, R43
46 Meyer, A. and Van de Peer, Y. (2005) From 2R to 3R: evidence for a fish-specific genome duplication. BioEssays **27**, 937–945

Received 17 January 2007/28 February 2007; accepted 6 March 2007
Published as BJ Immediate Publication 6 March 2007, doi:10.1042/BJ20070101